Petroleum Science 21 (2024) 551–566

Contents lists available at ScienceDirect

Petroleum Science

journal homepage: www.keaipublishing.com/en/journals/petroleum-science

Original Paper

Chemical modification of barite for improving the performance of weighting materials for water-based drilling fluids

Li-Li Yang [a, *], Ze-Yu Liu [a], Shi-bo Wang [a], Xian-Bo He [a], Guan-Cheng Jiang [a], Jie Zhang [b]

[a] MOE Key Laboratory of Petroleum Engineering, State Key Laboratory of Petroleum Resources and Prospecting, China University of Petroleum (Beijing), Changping District, Beijing, 102249, China
[b] MOE Key CNPC Drilling Research Institute, Changping District, Beijing, 102206, China

ARTICLE INFO

Article history:
Received 16 January 2023
Received in revised form
30 September 2023
Accepted 1 October 2023
Available online 3 October 2023

Edited by Jia-Jia Fei

Keywords:
Drilling fluids
Weighting materials
Filtration control
Reservoir protection
Stability property

ABSTRACT

With increasing drilling depth and large dosage of weighting materials, drilling fluids with high solid content are characterized by poor stability, high viscosity, large water loss, and thick mud cake, easier leading to reservoir damage and wellbore instability. In this paper, micronized barite (MB) was modified (mMB) by grafting with hydrophilic polymer onto the surface through the free radical polymerization to displace conventional API barite partly. The suspension stability of water-based drilling fluids (WBDFs) weighted with API barite:mMB = 2:1 in 600 g was significantly enhanced compared with that with API barite/WBDFs, exhibiting the static sag factor within 0.54 and the whole stability index of 2. The viscosity and yield point reached the minimum, with a reduction of more than 40% compared with API barite only at the same density. Through multi-stage filling and dense accumulation of weighting materials and clays, filtration loss was decreased, mud cake quality was improved, and simultaneously it had great reservoir protection performance, and the permeability recovery rate reached 87%. In addition, it also effectively improved the lubricity of WBDFs. The sticking coefficient of mud cake was reduced by 53.4%, and the friction coefficient was 0.2603. Therefore, mMB can serve as a versatile additive to control the density, rheology, filtration, and stability of WBDFs weighted with API barite, thus regulating comprehensive performance and achieving reservoir protection capacity. This work opened up a new path for the productive drilling of extremely deep and intricate wells by providing an efficient method for managing the performance of high-density WBDFs.

1. Introduction

Drilling fluids, the mixture of solids, liquids, and gases (Al-Darweesh et al., 2022), play an essential role in the safe and efficient drilling process (Jiang et al., 2021). As versatile circulation fluids, drilling fluids can suspend and remove cuttings (Mahmoud et al., 2020), balance the formation pressure (Elkatatny, 2019), lubricate the drill tools (Humood et al., 2019), transfer the hydraulic power (Gamal et al., 2019), reduce the heat (Kusrini et al., 2020), and so on. As deep and ultra-deep wells are increasingly frequently exploited, weighting materials have been used at a large scale to adjust the density (Jeennakorn et al., 2019), control downhole pressure, and stabilize the wellbore (Wang et al., 2020). For the high-density water-based drilling fluids (WBDFs), the stability (Wang and Xiong, 2022), rheology (Wang et al., 2022), filtration loss (Murtaza et al., 2021), wall-building (Liu et al., 2019), and lubricity, cannot be balanced and controlled at the same time. Particularly, the comprehensive performance regulation of high-density WBDFs still needs to be solved.

Barite is the most widely used as weighting agent (Leusheva et al., 2022) because of its high density (4.2–4.48 g/cm^3), moderate hardness, good stability, and non-magnetic and non-toxic. In recent years, researchers have searched for many new and alternative minerals, including limestone (Morenov et al., 2018), ilmenite (Basfar et al., 2019), magnetite (Almutawa et al., 2021), galena (Mao et al., 2020), Micromax (Gamal et al., 2022) and micronized barite (Conn et al., 2007). Due to the high cost, these weighting minerals have yet to be widely applied.

In high-density drilling fluids, solid particles account for vast volume. The enormous specific surfaces significantly reduce the

* Corresponding author.
E-mail address: yangll@cup.edu.cn (L.-L. Yang).

https://doi.org/10.1016/j.petsci.2023.10.001

free water through wetting and adsorption, resulting in high viscosity and structural force. The aggravation of particle sedimentation will result in a significant change in the density. As the drilling fluids circulate, the flow pressure sharply rises, probably leading to drilling accidents such as sticking, leakage, and even blowout (Liu et al., 2020), hindering subsequent operations. According to Felekoğlu's study (Felekoğlu, 2007), particle size distributions and morphologies of materials significantly affect rheology, filtration and other characteristics. The research and application of micronized particles of weighting materials are conducted to obtain better suspension stability by reducing particle size. The Stokes formula states that smaller particle size results in slower sag velocity and improved suspension stability (Huang et al., 2016). The viscosity of drilling fluids weighted with micronized particles increases rapidly at high density, due to the smaller size and increasing amount. Moreover, poor wall-building property leads to more water loss, and the micronized particles quickly invade the reservoir with filtrate to cause reservoir damage. Generally, researchers mix more than two weighting materials with different particle sizes (Wu et al., 2009; Basfar et al., 2019) in the high-density to balance the contradiction between rheology and suspension stability, improve the wall-building property and reduce costs by means of particle size grading, particle filling, and dense accumulation.

Anti-sagging agents were proposed to add into drilling fluids to mitigate barite settling. Zhang et al. (2017) synthesized the copolymer of ADBA as a tackifier and formed a 3D network structure which was built up through electrostatic interactions, hydrophobic association interactions, and hydrogen bonds. The WBDFs containing ADBA were capable of suspending the weighting particles and slowing down the sedimentation rate, and effectively controlled the rheology and filtration loss. Li et al. (2022) synthesized a gel former (WGA) using in WBDFs by free-radical polymerization. The solution adding WGA had 3D network structure, increased the hydrophobic force between molecular chains, and the network structure became denser, which could suspend the solid particles. High molecular anti-sagging polymer agents increase the viscosity of WBDFs, and suspend solid particles. In high-temperature and high-salt formations, it is easy to cause agents failure, and the particles will settle down due to viscosity reduction. Therefore, the suspension stability for weighting materials can be enhanced by changing the properties of solid particles.

In recent years, grafting modification of materials has also been a hot area in oil fields (Boakye and Mahto, 2021), and chemical modification of inorganic powder (Razmjou et al., 2011) is the most commonly applied. Through the chemical adsorption or chemical reaction on the surface, the materials can be modified, capable of withstanding high temperatures and salt, changing the properties, and enhancing the compatibility and dispersion. Various materials, including graphene oxide (Liu et al., 2021), SiO_2 (Jia et al., 2022; Wu et al., 2012), Fe_3O_4, and $CaCO_3$ (Shimpi et al., 2015), have been modified for applications as filtrate reducers, plugging materials, lubricants, tackifiers, and inhibitors, etc. Ao et al. (2021) synthesized a nano filtration additive with high-temperature resistance exceeding 240 °C and simultaneously high salinity tolerance by employing silica as the core and a zwitterionic polymer as the shell. Tian et al. (2019) introduced Fe_3O_4 nanoparticles grafted with poly acrylic acid/3-(trimethoxysilyl) propyl methacrylate into WBDFs to enhance the rheological and plugging performance. Tang et al. (2022) developed a high-temperature filtration reducer with a core-shell structure (PAASM-$CaCO_3$) using polymer in combination with nano-calcium carbonate, which the filtration loss was stable after aging at 200 °C.

Researchers have made significant efforts to modify barite to improve the compatibility and stability as a filler in coating (Sun et al., 2017), concrete, rubber (Ulusoy, 2019), medicine (Gillani et al., 2010), and other industries. The chemical modification of organic polymers on inorganic materials (Zou et al., 2008) can change the morphology, size, stability, and compatibility of inorganic materials and improve their versatility. Hu et al. (2014) fabricated hydrophobic barium sulfate aggregates with sodium cocoate as an anionic modifier, which weakened the surface polarity and varied it from hydrophilic to hydrophobic. Fang et al. (2014) synthesized surface functionalized $BaSO_4$ nanoparticles by combining in situ generation of SO_4^{2-} with the use of a difunctional surface modification agent. The modified $BaSO_4$ nanoparticles were used as filler in bone, effectively improving the bending modulus and compressive strength. It intrigued us to fabricate chemically modified barite to achieve a versatile additive in drilling fluids. According to the characteristics of drilling fluids, we selected appropriate monomers and reaction methods, optimized the synthesis parameters, and modified barium sulfate.

Herein, chemically modified micronized barite (mMB) grafted hydrophilic polymers was developed as weighting agents for WBDFs to test the properties of stability, rheology, filtration, lubricity, and reservoir protection. And the performance of the combination of mMB and API barite with the appropriate particle size distribution was also evaluated and compared as weighting materials in WBDFs. This material showed great potential as an additive in drilling to regulate multiple aspects of performance for WBDFs.

2. Experimental section

2.1. Materials

[2-(Methacryloyloxy)ethyl]dimethyl-(3-sulfopropyl)ammoniumhydroxide (MSAH, 99%), 2-acrylamide-2-methylpropane sulfonic acid (AMPS, 99%), N, N-dimethylacrylamide (stabilized with MEHQ, DMAA, 99%), N-vinylpyrrolidone (NVP, 99%), potassium persulfate ($K_2S_2O_8$, 99%) and barium chloride ($BaCl_2$, 99%) were purchased from Energy Chemical (China). Sodium bentonite (Na-Bent) was supplied by Weifang Huawei New Materials Technology Co., Ltd. (China). API barite (with an average diameter of 23 μm) and micronized barite (MB, with an average diameter of 1.7 μm) were purchased from Beijing Modern Oriental Fine Chemical Co., Ltd (China). A filtrate reducer (GBG) was developed by our laboratory, which is a zwitterion polymer. Other chemicals were obtained from Sinopharm Chemical Reagent Co., Ltd (China) and used directly without purification.

2.2. Modified micronized barite (mMB)

mMB was modified by a two-step route in an alkaline aqueous solution. In the first step, $BaCl_2$/MSAH mixed solution was added to MB suspension by vigorous stirring into a three-necked flask. Subsequently, the suspension was added dropwise with $K_2S_2O_8$/KOH solution and heated at 60 °C for 5 h. Then MB was modified with vinyl groups on the surface. In the second step, AMPS, DMAA, NVP, and the initiator $K_2S_2O_8$ were added sequentially into the solution. The mixture solution was charged with nitrogen to remove the oxygen and heated at 70 °C for 12 h. In order to achieve homogenous polymerization, we kept a certain stir speed to make MB fully dispersed in water during free radical polymerization, and it reduced the occurrence of self-polymerization. The resulting product was purified by centrifugation at 12,000 rpm, washed with deionized water to remove the unreacted monomers and the products of self-polymerization, repeated several times and separated out the deposition. The purified product was dried at 50 °C until the constant weight, then crushed into powder. The as-prepared white micro-sized barite particles (mMB) were obtained.

In addition, we synthesized polymers (PMADN) using the monomers mentioned above in a similar method, except that no vinyl-modified MB was added. The resultant copolymer was nominated as PMADN and used for comparison in the following study.

2.3. Formulation of weighted WBDFs

The Na-Bent dispersion (2 wt%) was used as the base fluid, in which GBG was added as a filtration additive, and KCl and $CaCO_3$ were added as clay stabilizers and plugging materials, respectively. Barite, including API barite, MB, and mMB, or the combinations, was used as weighing materials. The formulation of WBDFs was shown in Table 1.

2.4. Characterization of mMB

The powder of MB or mMB was dispersed in DI water through ultrasonication, with concentration of 10.0 g L^{-1}. The diluted suspension was dripped onto the platform with conductive adhesive attached, dried in the air, and sprayed with platinum before observation. The micromorphologies of samples were observed by scanning electron microscopy (SEM, SU8010, Hitachi, Japan). We also used transmission electron microscopy (TEM, JEM-2100 F, FEI, USA) to observe the micromorphologies of samples. The diluted suspension was dripped onto a carbon film and dried in the air.

The chemical structures and functional groups of PMADN, MB, and mMB were tested by Fourier transform infrared spectrometer (FTIR, Nicolet 6700, Thermal Scientific, USA) within the range of 4000 to 400 cm^{-1}.

The thermal stabilities of PMADN, MB, and mMB were tested by a thermogravimetric analyzer (TGA, Q 600 SDT, Netsch, Germany) within the range of 25–600 °C.

The particle size distribution of API barite, MB and mMB dispersion, and WBDFs weighted with each weighting material were measured by laser particle size analyzer (Bettersize, 2000; Horiba, Japan). The ζ potentials of samples were tested by ζ potential analyzer (Zeta sizer Nano ZS, Malvern, UK).

2.5. Sag stability evaluation

2.5.1. Suspension stability test in water

Equal amounts of MB and mMB were dispersed in DI water through ultrasonication, and stood until the particles completely settling to the bottom, to test the suspension stability of each weighting material.

2.5.2. Static sag test

The static sag test was performed for WBDFs containing different weighting materials after aging at 180 °C for 16 h and standing for 1 h, and 10 mL of the top and bottom suspension were taken out to determine the density. The static sag factor (SF) was calculated according to the formulation shown in Eq. (1):

$$SF = \frac{\rho_{bottom}}{\rho_{top} + \rho_{bottom}} \tag{1}$$

where ρ_{bottom} and ρ_{top} were the bottom and top densities of drilling fluids, g·cm^{-3}, respectively. An *SF* between 0.50 and 0.53 (Wagle et al., 2018) indicated that the static settlement of drilling fluid had not occurred, while a higher *SF* than 0.53 meant that static settlement of drilling fluid had occurred.

2.5.3. In-time monitoring of stability in WBDFs

The static stability of weighted WBDFs was characterized by using a stability analyzer (Turbiscan LAB, Formulaction, France). This instrument (Ren et al., 2018; Delforce et al., 2021) applied the principle of static multiple light scattering to digitally observe the change of sample concentration or particle size by the change of transmitted or backscattering light intensity. Turbiscan stability index (TSI) were used to quantify the stability of samples and the formulation was shown in Eq. (2):

$$TSI = \sum_i \frac{\sum_h |\mathrm{scan}_i(h) - \mathrm{scan}_{i-1}(h)|}{H} \tag{2}$$

where *h* and *H* were the selected height and the total height of the sample, respectively. A larger *TSI* represented a less stable system, whereas a smaller *TSI* indicated a more stable system.

2.6. Rheological properties of weighted WBDFs

We used an electrical 6-speed viscometer (Qingdao Tongchun Petroleum Instrument Co., Ltd., China) to determine the rheology of WBDFs. We referred to China Petrochemical Industry Standard SY/T 5621-93 for the measurement and recorded the values at different rates of 600, 300, 200, 100, 6, and 3 rpm. *AV*, *PV*, and *YP* were calculated by the following equations:

$$AV = 0.5\theta_{600} \tag{3}$$

$$PV = \theta_{600} - \theta_{300} \tag{4}$$

$$YP = 0.511(\theta_{300} - PV) \tag{5}$$

where *AV* was the apparent viscosity of WBDFs, mPa·s; *PV* was the plastic viscosity of WBDFs, mPa·s; and *YP* was the yield point of WBDFs, Pa.

2.7. Filtration performance of weighted WBDFs

The API filtration loss was measured by the API filtration apparatus (Qingdao Haitongda Special Instrument Co., Ltd., China) at 0.7 MPa for 30 min. And the HTHP (high-temperature high-pressure) filtration loss was tested by the HTHP filtration apparatus (Qingdao Tongchun Special Instrument Co., Ltd., China) at 3.5 MPa under 150 °C for 1 h. The filtration volume was recorded and the freshly prepared filter cakes were dried naturally in the air.

2.8. Lubricity of weighted WBDFs

2.8.1. Mud cake sticking test

A mud cake sticking tester (NZ-3, Qingdao Xinsen Electromechanical Equipment Co., Ltd., China) was used to determine the lubricity of the as-prepared mud cake. Under the condition that the worktable was inclined, the sliding block placed on the mud cake was subjected to downward gravity and started sliding after

Table 1
Formulation of WBDFs.

Formulations	Dosage	Function
Na-Bent	2 wt%	Viscosifying
Na_2CO_3	2 wt‰	Promoting Na-Bent dispersion
GBG	5 wt%	Filtrate reducer
KCl	5 wt%	Shale inhibitor
$CaCO_3$	5 wt%	Plugging
Barite		Weighting material
Water		Disperse medium

overcoming the viscous force. The sticking coefficient of the mud cake was calculated as follows:

$$\text{Sticking coefficient} = \tan\alpha \tag{6}$$

where α was the flip angle.

2.8.2. Four-ball friction test

The four balls friction test (MRS-100 Four-Ball Friction Tester) was used to evaluate the long-term wear resistance of the weighted drilling fluid according to the friction coefficient and wear marks. We referred to China Petrochemical Industry Standard SH/T 0189 for the measurement. A load in the axial direction at 147 N was applied to drive the upper ball to rotate at a set speed (600 r/min) and produce relative sliding with the three steel balls and the friction coefficient was measured for 900 s. After the test, the wear marks on the surface of the steel balls were observed with digital images.

2.9. Core damage experiment

A JHMD-2 high-temperature high-pressure core dynamic contaminator (Qingdao Xinsen, China) was used to assess the reservoir protection of the weighted drilling fluid. We used the artificial cores which were prepared by cementation and compaction of quartz sand with epoxy resin, and mixed with clay particles. The diameter, length, and dry weight of the core were measured in advance (Table 2). We referred to China Petrochemical Industry Standard SY/T 6540-2002 for the measurement. We used kerosene with viscosity of 2.2 mPa·s for core displacement and set the confining pressure of 4 MPa, a flow rate of 2 mL/min, and the core polluted with WBDFs for 2 h at room temperature. The permeability and permeability recovery rate of the core were calculated as follows:

$$K = 0.1\frac{Q\mu L}{A\Delta p} \tag{7}$$

where K was the permeability of the core, μm^2, 1 μm^2 = 1.013*10^3 mD; Q was the flow rate of kerosene, cm^3/s; μ was the fluid viscosity, mPa·s; L was the length of the core, cm; A was cross section area, cm^2; Δp was pressure difference, MPa.

$$R = \frac{K_{od}}{K_o} \tag{8}$$

where R was the permeability recovery rate of the core; K_o was the permeability before pollution, mD; K_{od} was the permeability after pollution, mD.

3. Results and discussion

3.1. Characterization of mMB

In this study, mMB was modified by a two-step route (Fig. 1). In the first step, MB (Fig. 2(a)) was modified with MSAH as a surface modifier with bifunctional groups to produce vinyl and quaternary ammonium functionalities, by barium ion complexed with the sulfonic group of MSAH. In alkaline solution, the MB surface was electronegative and adsorbed with barium ion. Potassium persulfate slowly decomposed into sulfate at 60 °C, and reacted with barium ion to form barium sulfate, deposited on the MB. The second step (Fig. 2(d)) was grafting with AMPS, DMAA, and NVP on the vinyl functionalized MB. AMPS contained strong anionic and water-soluble sulfonic acid groups to improve the dispersion stability and hydration ability. The copolymers containing AMPS could reduce filtration loss and improve the rheology of drilling fluid (Huang et al., 2019). DMAA had a hydrophilic amide group, which had good hydrolysis resistance. NVP had rigid pyrrole rings which can improve the stability and thermal resistance of the polymer. SEM and TEM observations exhibited rough surface with edges and corners for MB particles (Fig. 2(b) and (c)). And a flat and smooth surface was generated on mMB (Fig. 2(e) and (f)) after modification. The density of MB was 4.2 g/cm^3, and about 0.1 g hydrophilic polymers was grafted onto 1 g MB particles. The density of mMB was slightly smaller than that before modification.

After intense agitation and ultrasonic treatment, API barite, MB and mMB were dispersed in water. API barite particles deposited entirely in just 1 min, and MB deposited in 5 min. The dispersion of mMB was maintained stable for 6 h. The ζ potential of API barite, MB, and mMB was −3.8, −11.5, and −26.9 mV (Table 3). Compared with MB, the ζ potential of mMB was higher because of the successful modification. According to DLVO theory, MB easily agglomerated in water, probably due to its large specific surface area and long-range interaction, while mMB could enhance the suspension stability through electrostatic repulsion and steric hindrance.

The FTIR (Fig. 2(g)) technique was adopted to determine the surface composition of mMB. 3447 cm^{-1} was the stretching vibration absorption peak of N–H on secondary amide. 2977 and 2934 cm^{-1} were the stretching vibration of methyl (–CH_3) and methylene (–CH_2–) groups. 1634 cm^{-1} was the vibration absorption peak of the C=O bond in the amide group. 1549 cm^{-1} was the bending vibration peak of N–H. 1463 cm^{-1} was the characteristic absorption peak of the C–N^+ group in MSAH. 1444 cm^{-1} was the C–N stretching vibration peak. 1442 cm^{-1} was the asymmetric bending vibration peak of C–H, and 1368 cm^{-1} was the symmetric bending vibration peak of C–H. 1317 cm^{-1} was the characteristic absorption peak of C–N. 1181, 1084, and 636 cm^{-1} were the distinct absorption peaks of –SO_3H. There is no characteristic absorption peak of C=C in the range of 1675–1640 cm^{-1}, indicating that all monomers participated in the polymerization reaction. The peak of 1119, 983.04, and 611.81 cm^{-1} were the characteristic absorption peaks of barite.

The TGA curves of PMADN, MB, and mMB were shown in Fig. 2(h). MB only lost physically adsorbed water when the temperature increased. The onset temperature of mMB was 366 °C. It showed the positive influence of the inorganic component on thermal stability since the onset temperature of PMADN was 323 °C. The total weight loss was 5 wt% for mMB, slightly lower than the content of monomers because of the incomplete polymerization, removal in purification, and deposition of the sulfonate group onto MB together with barite ions.

Table 2
Properties of the cores used in core damage experiment.

Core	Diameter, mm	Length, mm	Gas permeability, mD	Median diameter of pore throat, μm
1	2.53	5.111	147.77	0.323
2	2.51	5.432	152.66	0.752
3	2.52	5.322	156.23	0.544

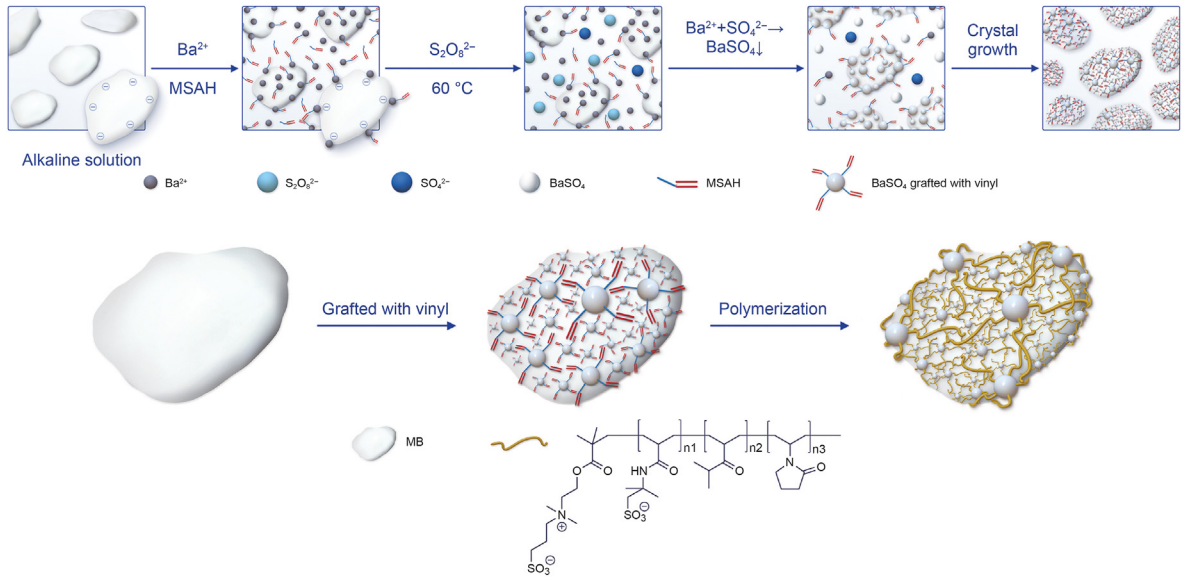

Fig. 1. Schematic illustration of the modification route of mMB.

The particle size distribution of different weighting materials in water was measured (Fig. 2(i)). API barite was in a broad particle size distribution, in which coarse particles (greater than 10 μm) accounted for more than 70%, fine particles (less than 5 μm) accounted for less than 10%, and the average particle size was 23 μm. The particle size distribution of MB and mMB ranged from 1 to 5 μm with an average size of 2.41 and 2.83 μm, exhibiting a narrow particle size distribution. The mMB after modification with a grafted polymer film was slightly larger than MB.

3.2. Sag stability evaluation

The suspension of MB and mMB in water was shown in Fig. 3. The particles of MB completely settled down to the bottom within 5 min, and the suspension property was poor. The settling speed of mMB decreased significantly, and the particles completely settled down after standing for 6 h. The suspension stability of modified mMB was excellent compared with that before modification.

To achieve the expected densities, dosages of 300, 400, 500, and 600 g were added into WBDFs in this study to densities of 1.47, 1.60, 1.71 and1.82 g cm^{-3}, respectively (Fig. 4(a)).

The vertical static sag test was conducted at room temperature after aging at 180 °C for 16 h and standing for 1 h. For API barite/WBDFs, the density difference (Fig. 4(b)) increased from 0.629 to 0.655 g cm^{-3} with the dosage increasing from 300 to 600 g, and the SF (Fig. 4(c)) increased from 0.629 to 0.655, far exceeding the safe value of 0.53. Regarding the WBDF weighted with MB, the corresponding density difference changed from 0.301 to 0.371 g cm^{-3}, and the SF changed from 0.534 to 0.568, slightly exceeding the safe level. Comparatively, the density difference of mMB/WBDFs varied from 0.128 to 0.14 g cm^{-3}, and the SF varied from 0.517 to 0.529. Therefore, only mMB made WBDFs remain within the safe range with increasing dosage. A combination of API barite and mMB was also used as the weighting materials. In the case of API barite/mMB ratio of 2:1, the density difference increased from 0.211 to 0.302 g cm^{-3}, and the SF rose from 0.529 to 0.545 with the dosage increasing from 300 to 600 g. It can be seen that the partial substitution of API barite with mMB slowed down the settling speed of solid particles, enhanced the stability of the system.

We also assessed the in-time stability of WBDFs by monitoring the backscattering light intensity at different heights. For API barite/WBDFs (Fig. 5(a) and (b)), with the extension of the settling time, the backscattering light intensity at the top decreased significantly, and the intensity at the bottom increased on the contrary. After standing for 6 h, a deposition layer with a thickness of 6 mm was formed, and the top appeared stratification with a height of 5 mm. The light intensity fluctuated strongly at the middle layer ranging from 5 to 20 mm, indicating that the solid particles gradually dropped from the upper layer to the middle until the bottom. The overall TSI was 3.4 (Fig. 5(e)) after 6 h, the TSI of top layer was 7.5, the middle was 2.5, and the bottom was 2.0. It showed every layer of the system was unstable.

For the case of API barite/mMB ratio of 2:1 (Fig. 5(c)–(d)), the backscattering light intensity at the top decreased which observed water layer separated out with a height of 1 mm. The intensity was slightly enhanced within the range of 0–2 mm at the bottom, which indicated the concentration of particles at the bottom was slightly increased instead of deposition. There was no significant change in light intensity for the middle layer, and the range of 1–26 mm for WBDFs was stable. The overall TSI was 1.9 after 6 h (Fig. 5(f)), and the system stability had been greatly improved compared with API barite/WBDFs.

The phenomenon also evidenced the stability after standing for 1 d that API barite/WBDFs (Fig. 6(a)–(b)) exhibited more severe stratification, and the top layer turned shallow and the solid deposition was discerned. In contrast, the one weighted with API barite/mMB (Fig. 6(c)–(d)) ratio of 2:1 exhibited slight water separation.

Combined with the ζ potential and physical characteristics, due to the existence of polymer film of mMB, the hydration volume of particles was increased, and buoyancy was slightly increased. Negatively charged polymers supplied electrostatic force and steric hindrance, prevented the particles adsorption and aggregation. In addition, the suspension stability of mMB/WBDFs also originated from the enhanced interaction among polymer segments and clays. When API barite and mMB were mixed into WBDFs, the solid particle precipitation rate was slowed down and the wellbore stabilization was improved.

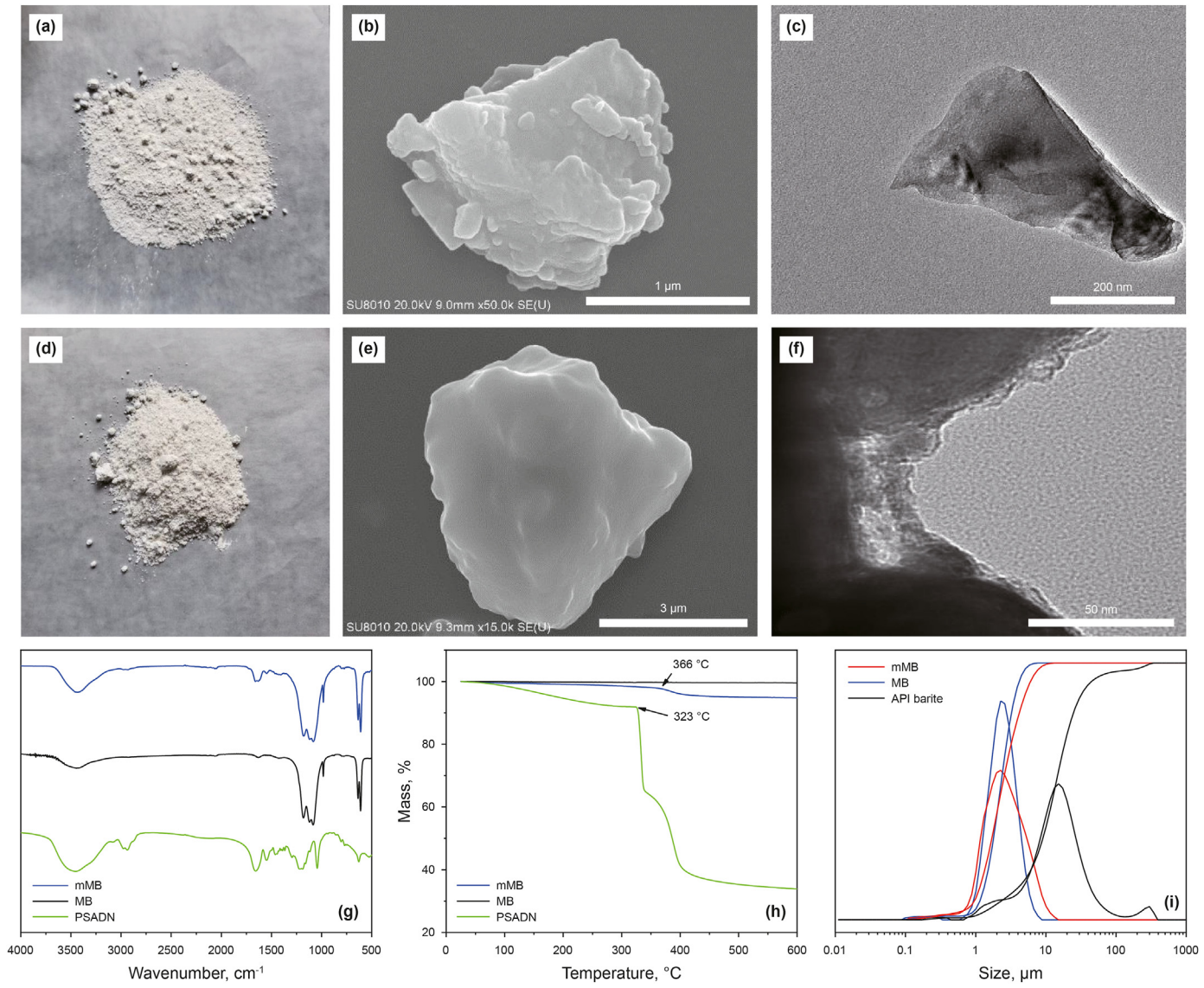

Fig. 2. (**a**–**c**) Photograph, SEM image, and TEM image of MB, respectively; (**d**–**f**) photograph, SEM image, and TEM image of mMB, respectively; (**g**) FTIR spectra of mMB, MB, and PMADN. (**h**) TGA curves of mMB, MB, and PMADN; (**i**) particle size distributions of API barite, MB and mMB dispersions in water.

Table 3
ζ potential of each formulation measured at 25 °C.

Barite type	ζ potential, mV
API barite	−3.8
MB	−11.5
mMB	−26.9

3.3. Rheological properties of WBDFs

We studied the effect of the type, dosage and proportion of mixture on the rheology of WBDF before and after aging at 180 °C for 16 h. Results showed that when the dosage increased from 300 to 600 g, AV (Fig. 7(a)) increased substantially, from 70 to 105 mPa·s for API barite/WBDFs, from 68 to 121 mPa·s for MB/WBDFs, and from 85 to 155 mPa·s for mMB/WBDFs before aging. The similar increasing trend applied for PV (Fig. 7(b)) and YP (Fig. 7(c)), and AV after aging. Additionally, viscosity and yield point of mMB/WBDFs were higher than that of MB/WBDFs and API barite/WBDFs at the same dosage before and after aging, positively impacted the system's stability. When a combination of API barite and mMB was added into WBDFs, the viscosity decreased initially and then increased with increasing the API barite/mMB ratio, irrespective of the total dosage. When the ratio was 2:1, all rheological parameters reached the minimum value, 60 mPa·s in AV (Fig. 7(d)), 48 mPa·s in PV (Fig. 7(e)), 12 Pa in YP (Fig. 7(f)) before aging, and 35 mPa·s in AV, 28 mPa·s in PV and 7 Pa in YP after aging. Therefore, the rheological properties can be improved by optimizing the API barite/mMB ratio.

The viscosity was interpreted as follows. At low density, solid particles dispersed in WBDFs, and viscosity was dominated by solid-liquid friction. There was little difference in rheological properties for WBDFs weighted with different weighting materials. As the density increased, the solid content increased rapidly, the distance between particles decreased sharply, and the likelihood of particles contacting each other increased, which led to the dramatic increasing friction between solid-solid phases, and thus the viscosity increased. MB and mMB had more numbers of particles compared with API barite. The network formed between the

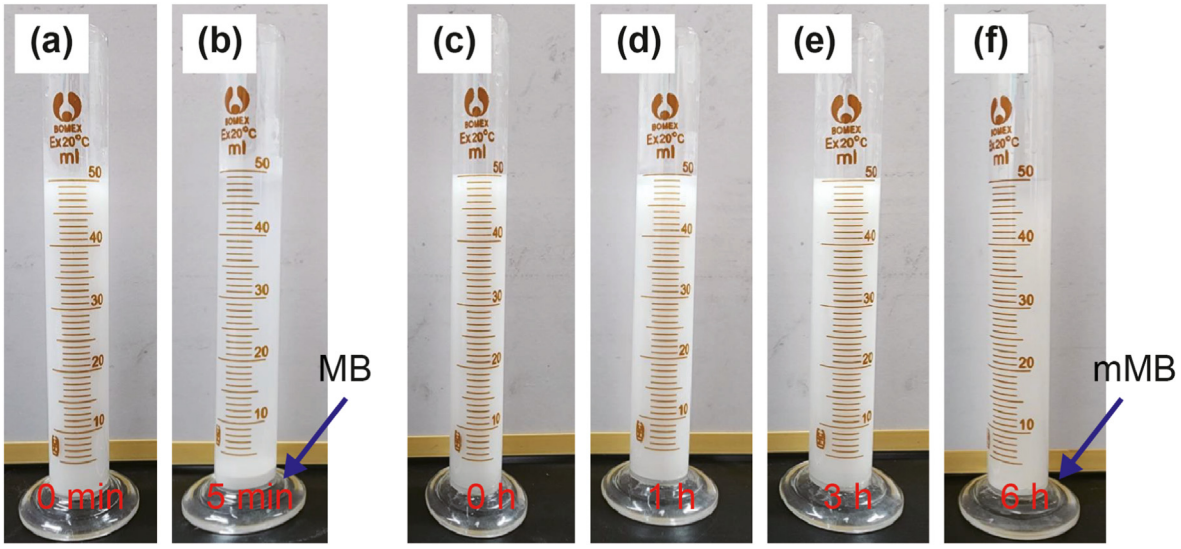

Fig. 3. (**a**–**b**) MB and (**c**–**f**) mMB dispersions in water.

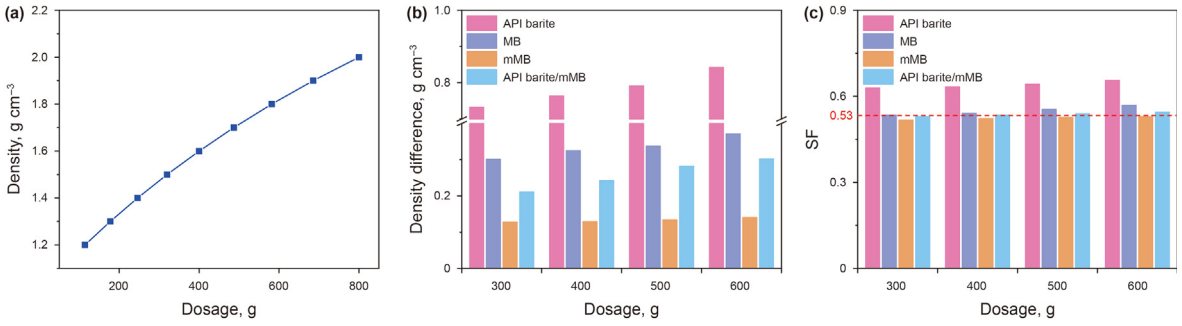

Fig. 4. (**a**) Relation curve between the density of WBDFs and dosage of weighting materials. (**b**) The density difference between the upper and lower layers of WBDFs weighted with different barites after aging at 180 °C for 16 h and standing for 1 h. (**c**) The SF in the vertical position of WBDFs weighted with different barites after aging at 180 °C for 16 h and standing for 1 h.

particles in WBDFs (Navarrete et al., 2022) and it was supposed to arise from the short-range repulsive forces (Faraudo and Bresme, 2005), preventing the free flow. For mMB, the entanglement and intermolecular interaction of the grafted polymer on the surface increased the viscosity further.

The viscosity reduction of WBDFs after adding the combination of different materials with different sizes was as follows (Fig. 8). The solid particles were stacked by the strong friction, collision, and extrusion, forming a stable structure. The addition of mMB (fine particles) weaken these physical interaction, thus reducing the viscosity of WBDFs (Xu et al., 2019). When mMB was added, the mMB distributed around API barite, leading to the relatively less contact between large particles and decreased the viscosity. It seemed that fine particles in the flow had a lubricating effect. Other researchers had also found a similar phenomenon in the industry of coal (Das et al., 2020), food, and construction (Kabagire et al., 2019). The ratio of API barite (coarse particles) and mMB (fine particles) with 2:1 was continuously distributed. According to the dense packing principle (Wang et al., 2022), the larger the packing density and the smaller the void fraction compared to API barite only, the better rheology of high-density WBDFs. However, the viscosity would increase with increasing the percentage of fine particles. After aging, the WBDFs maintained good rheological properties.

3.4. Filtration control performance of WBDFs

The water in WBDFs easily penetrates the formation under high pressure. Weighting materials balance the formation pressure and cooperate with Na-Bent and other additives to mitigate fluid intruding into the reservoir by forming a mud cake.

The filtration volumes of WBDFs weighted with API barite, MB, and mMB after aging at 180 °C for 16 h were measured. As the dosage increased from 300 to 600 g, API filtration volume for API barite/WBDFs (Fig. 9(a)) increased from 1.3 to 1.8 mL, and HTHP filtration volume (Fig. 9(b)) increased from 18 to 22 mL, showing the negative impact of high temperature and high pressure on the filtration. Compared to MB/WBDFs, the API filtration volume of mMB/WBDFs decreased by more than 80%, and HTHP filtration volume decreased by more than 25% under different dosages from 300 to 600 g.

The relationship between HTHP filtration loss of different WBDFs and $t^{1/2}$ was depicted in Fig. 9(c). The initial filtration rate of the API barite/WBDFs was less than that of mMB/WBDFs due to the quick bridging effect of API barite. In comparison, the slow settling speed of mMB led to the slow formation speed of mud cake and high instantaneous filtration loss. After 2 min, the filter cake had been initially formed and the subsequent filtration rate tended to be the same.

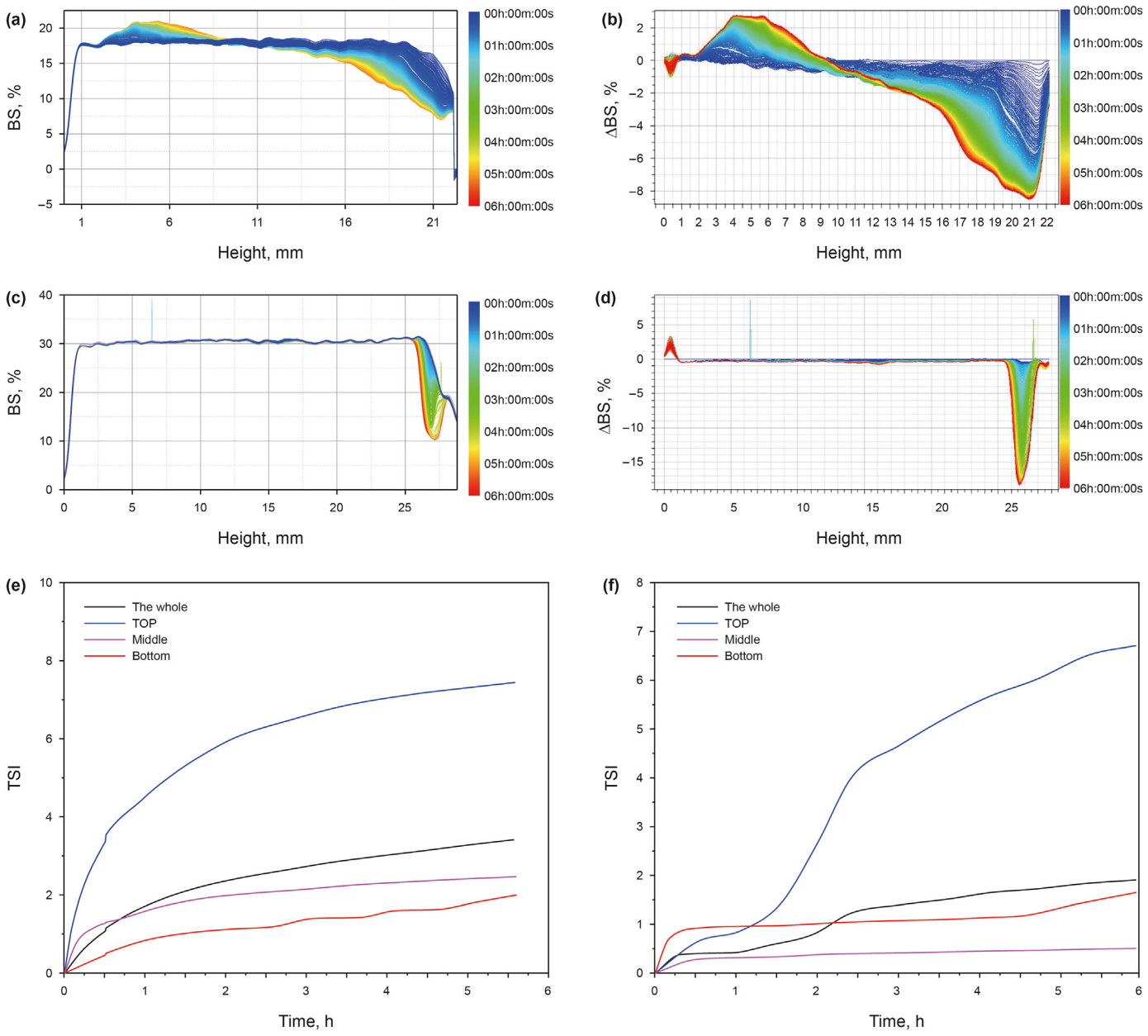

Fig. 5. (**a**, **b**) Backscattering signal and Delta backscattering signal of WBDFs weighted with API barite scanned for 6 h at different heights, (**c**, **d**) Backscattering signal and Delta backscattering signal of WBDFs weighted with API barite:mMB = 2:1 scanned for 6 h at different heights. TSI of WBDFs weighted with (**e**) API barite and (**f**) API barite:mMB = 2:1.

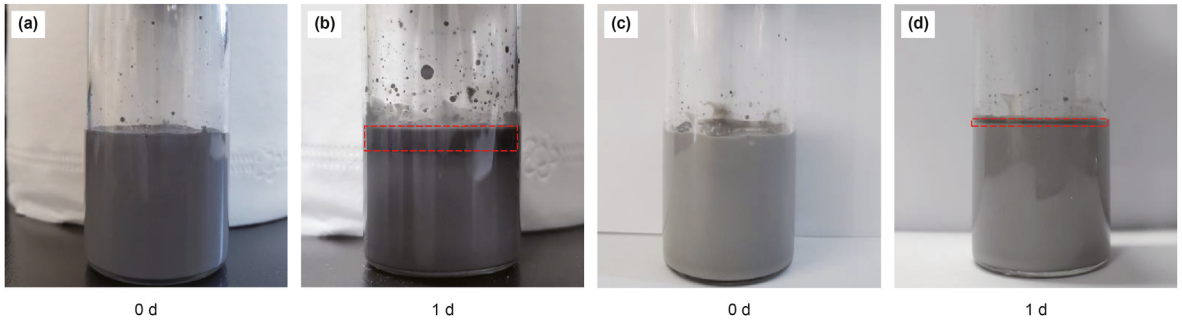

Fig. 6. Images of WBDFs weighted with (**a, b**) API barite standing for 0 and 1 d at room temperature, (**c, d**) API barite:mMB = 2:1 after aging at 180 °C for 16 h, and those standing for 0 and 1 d at room temperature.

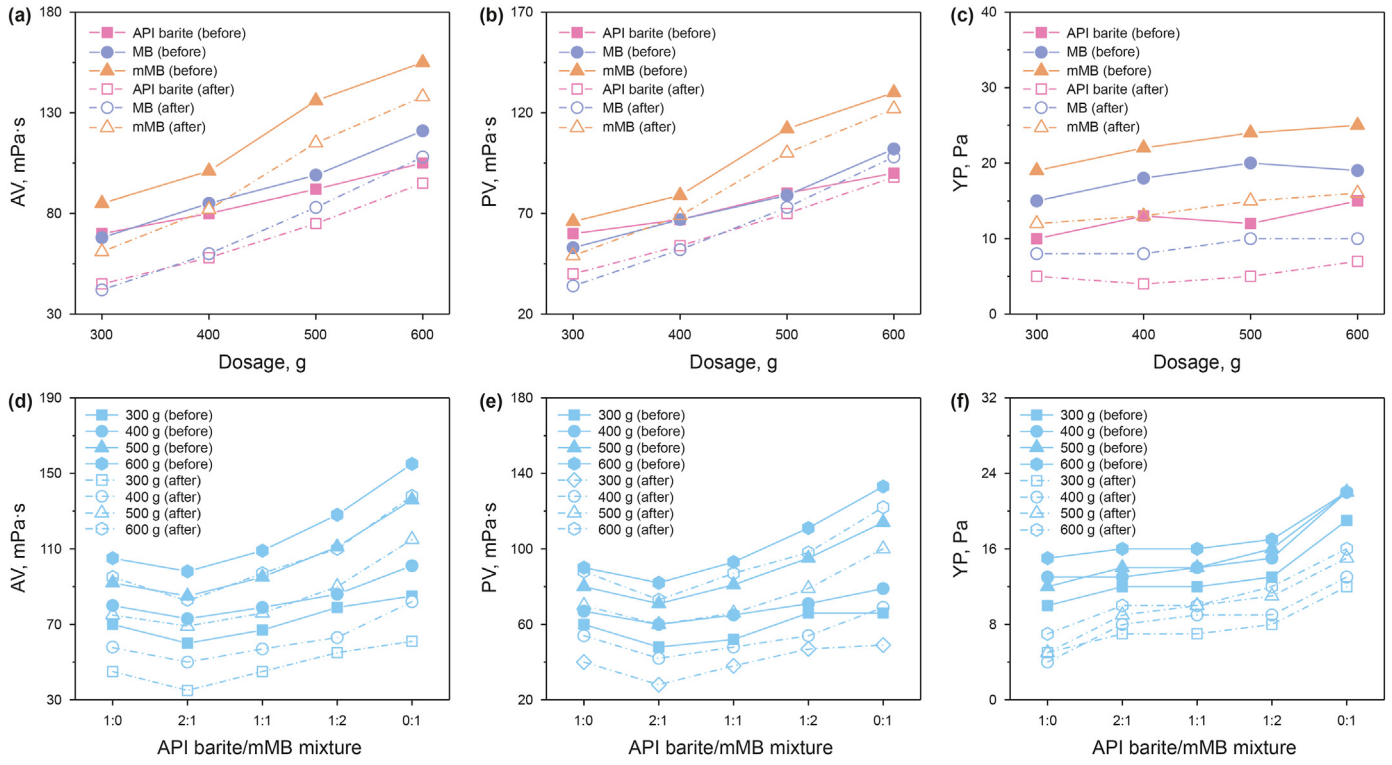

Fig. 7. (**a**) AV, (**b**) PV, and (**c**) YP of WBDFs weighted with different dosages of API barite, MB or mMB before or after aging at 180 °C for 16 h. (**d**) AV, (**e**) PV, and (**f**) YP of WBDFs weighted with combinations of API barite and mMB at different ratios before or after aging at 180 °C for 16 h.

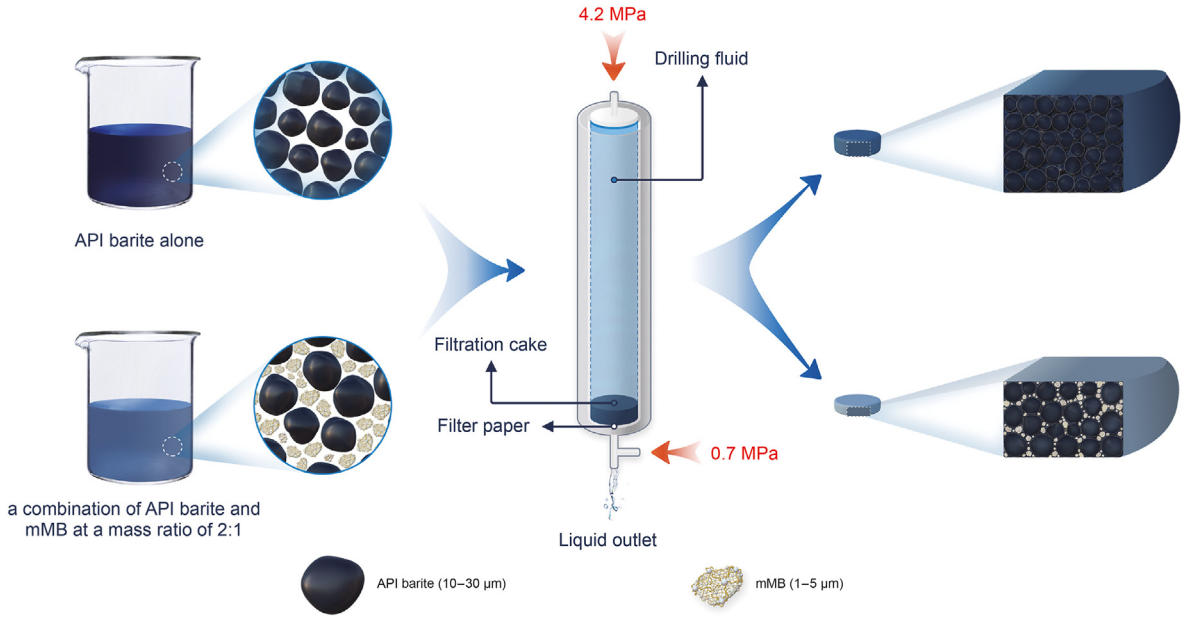

Fig. 8. Mechanism of WBDFs weighted with a combination of API barite/mMB in regulating rheological properties and filtration performance.

The filtration loss of WBDFs weighted with different combinations of different weighting materials at a dosage of 400 g with a ratio of 1:1 was evaluated (Fig. 9(d)). For the combinations of API barite/MB and API barite/mMB, API filtration volumes were 2.2 and 1.4 mL, and HTHP filtration volumes were 26 and 24 mL, respectively. The filtration loss of API barite/MB was larger than that of API barite/mMB. In contrast, chemically modified API barite was prepared in the same method as mMB and used to displace with API barite to be mixed with MB or mMB. The API filtration volume was 1.4 and 1.2 mL, respectively, and HTHP filtration volume were both 22 mL. Therefore, the grafted hydrophilic polymer decreased the pore numbers and sizes, and improved the quality of mud cake.

The filtration losses of WBDFs weighted with API barite and mMB at different ratios were assessed (Fig. 9(e) and (f)). When API barite:mMB = 2:1 at 300 g, the filtration losses were 1.3 (API filtration) and 19 mL (HTHP filtration), and when the total dosage

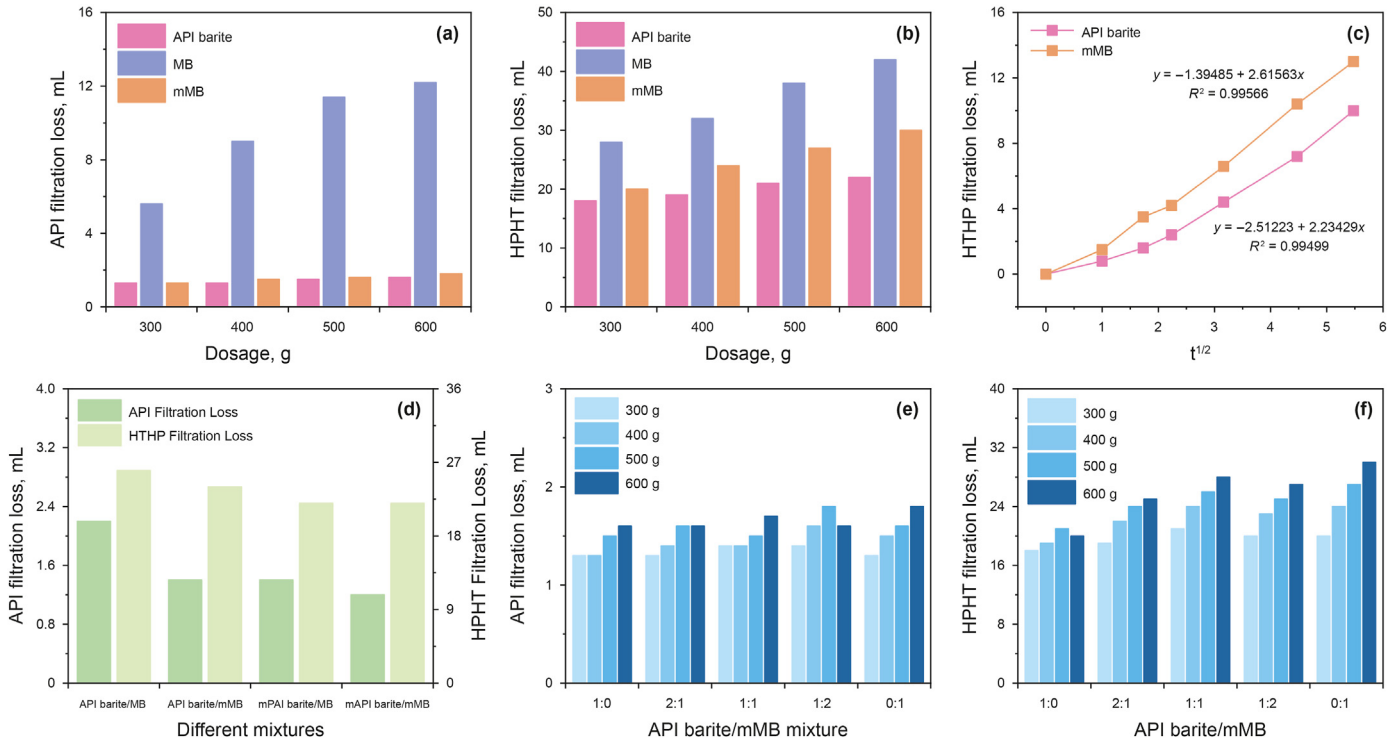

Fig. 9. (**a**) API filtration loss and (**b**) HTHP filtration loss of WBDFs weighted with different dosages of API barite, MB and mMB after aging at 180 °C for 16 h. (**c**) Relationship between filtration loss of WBDFs aging at 180 °C for 16 h and $t^{1/2}$. (**d**) Filtration loss of WBDFs weighted with different combinations of weighting materials after aging at 180 °C for 16 h. (**e**) API filtration loss and (**f**) HTHP filtration loss of WBDFs weighted with API barite and mMB at different ratios after aging at 180 °C for 16 h.

increased to 600 g at the same ratio, the filtration loss were 1.6 (API filtration) and 25 mL (HTHP filtration). Therefore, the combination of API barite and mMB at a ratio of 2:1 exhibited a lower filtration loss.

API barite was easy to settle down, and under a certain pressure difference, mud cake could be quickly formed which decreased the filtration volume (Fig. 8). API barite/WBDFs showed a bimodal distribution (Fig. 10 and Table 4) which contributed to the less filtration loss. The particle size distribution of mMB/WBDFs showed a unimodal peak. Particles of mMB had better suspension stability and could not immediately settle down, thus were unable to block

Table 4
Median particle size and average particle size of different weighting materials in water and WBDFs.

Barite type	Solution	D_{50}, μm	D_m, μm
API barite	Water	13.159	22.937
MB	Water	2.218	2.409
mMB	Water	2.302	2.839
API barite	WBDF	9.249	30.689
MB	WBDF	2.495	2.817
mMB	WBDF	2.334	2.722

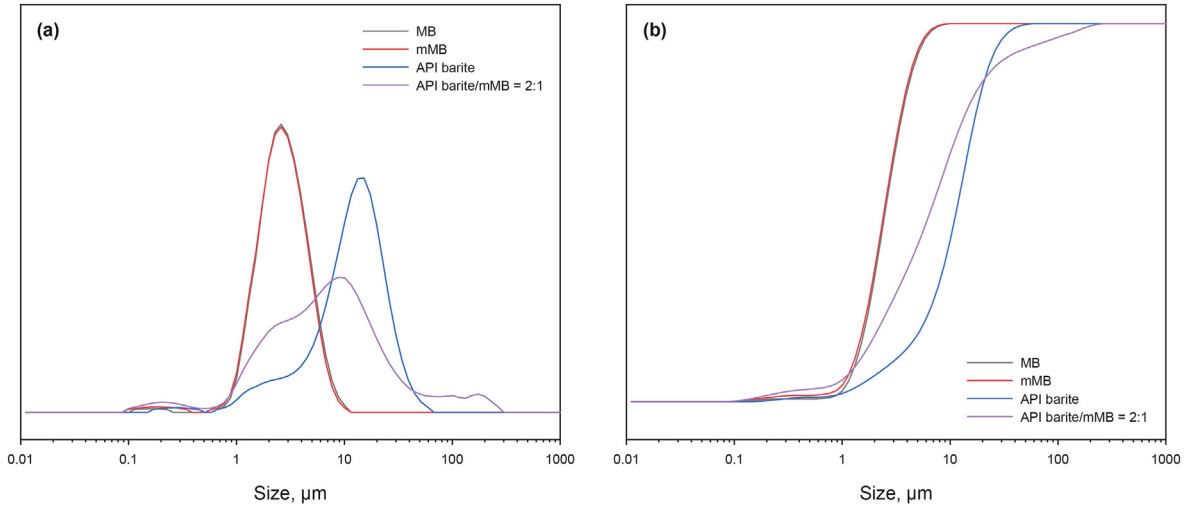

Fig. 10. Particle size distribution of WBDFs weighted with API barite, MB, mMB and API barite:mMB = 2:1.

the pores promptly, resulting in large filtration loss. In addition, the filtrate of MB/WBDFs was opaque, indicating that the pores of the mud cake were large enough for MB particles to penetrate through. For mMB/WBDFs, the adsorption of grafted polymers of mMB onto clay particles and the fill-in effect of fine particles were favorable to form a compact mud cake and block the pores, resultantly reducing the filtration.

For API barite:mMB = 2:1/WBDFs, It shows a wider particle size distribution and smaller average (D_m) and median particle sizes (D_{50}) (Fig. 10 and Table 4), compared with API barite/WBDFs. Some API barite coarse particles settled to the bottom first and formed primary mud cake, and mMB fine particles were filled in the gaps

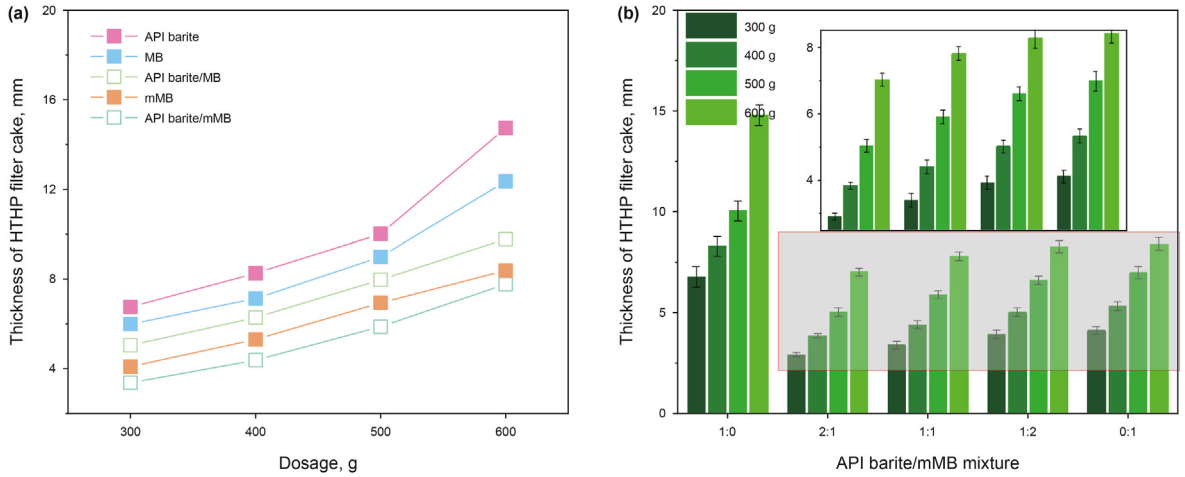

Fig. 11. (**a**) Thicknesses of freshly prepared mud cakes of WBDFs weighted with different weighting materials in HTHP filtration after aging at 180 °C for 16 h. (**b**) Thicknesses of freshly prepared HTHP mud cakes of WBDFs weighted with API barite and mMB at different ratios after aging at 180 °C for 16 h.

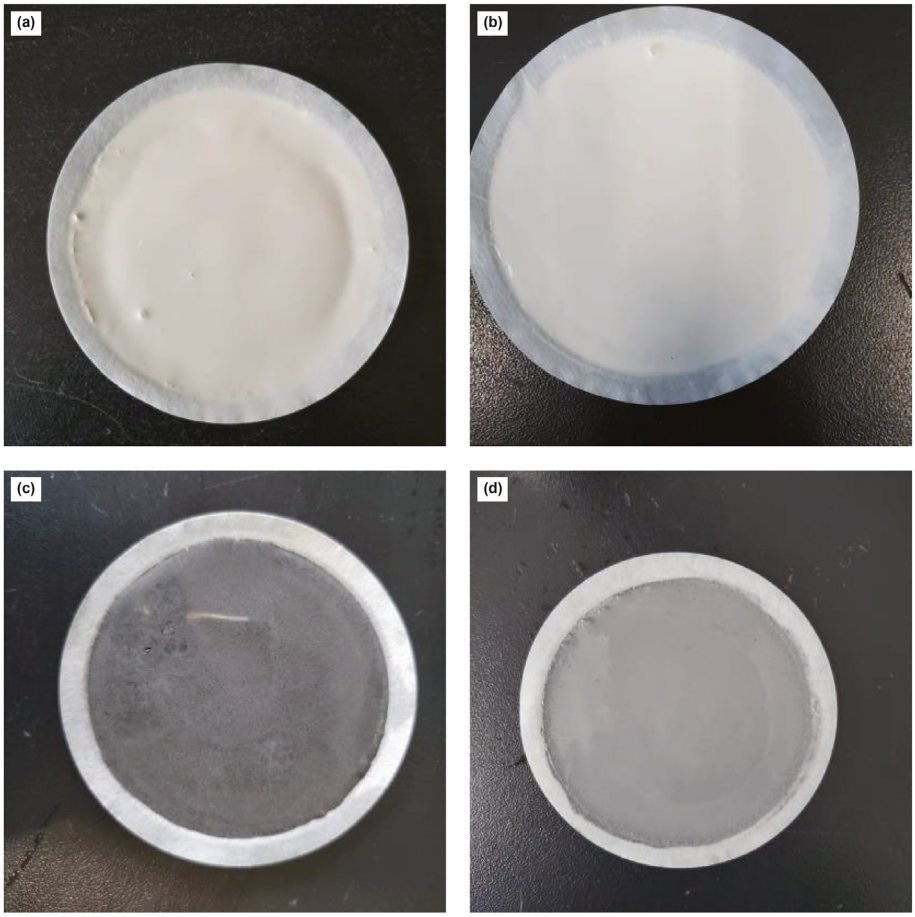

Fig. 12. Digital images of freshly prepared mud cakes of WBDFs weighted with weighting materials after aging at 180 °C for 16 h. (**a**) 600 g of MB, (**b**) 600 g of mMB, (**c**) 600 g of API barite, (**d**) 600 g of API barite:mMB = 2:1.

between coarse particles. Due to the grafted polymers, the holes were further filled. Weighting materials and clays formed multi-stage filling, promoted the dense accumulation and improved the quality of the mud cake. Coarse particles played the role of bridging, and fine particles filled in the gaps, improving the bulk denseness and reducing the pores. Therefore, an appropriate ratio of grafted fine particles in WBDFs was demonstrated to enhance the filtration performance and wellbore stabilization.

3.5. Characteristics of mud cakes

3.5.1. Morphologies of mud cakes

The quality of the filter cakes reflects the filtration performance. Accordingly, we measured the thickness of filter cakes of WBDFs weighted with different weighting materials (Fig. 11) and observed the microscopic images (Figs. 12 and 13).

With the increase of weighting materials, the solid content in the WBDFs increased significantly, and the mud cake was thicker. The thickness of mud cake for API barite/WBDFs increased from 6.75 to 14.74 mm with the dosage increasing from 300 to 600 g. For MB/WBDFs, the thickness increased from 5.99 to 12.36 mm. For mMB/WBDF, the thickness increased from 4.09 to 8.38 mm, with a reduction of 31% compared with MB/WBDFs.

API barite particles were large and were quickly deposited at the bottom, causing the incompact accumulation and stacked disorderly (Fig. 14(a)). It formed a thick mud cake and promptly impeding the subsequent filtration process. The thickness of mud cake was the largest. With the increase of dosage, more particles settled down with stacked in disorder, and the largest increase of thickness for API barite/WBDFs. SEM images (Fig. 13(a)) showed the mud cake had large size of pores. MB was easy to agglomerate. The particle size distribution was concentrated and the mud cake for MB/WBDFs had many pores (Fig. 13(b)), which could not prevent water loss. The particles of mMB were dispersed well and interacted with clays due to grafted polymer to reduce the porosity of mud cake with small size pores (Fig. 13(c)). The thickness was thinner, and the increase of thickness increased slowly.

The thickness of the mud cake for WBDFs weighted with the mixture of API barite and mMB primarily decreased and then increased slowly with the increase of the ratio of API barite and mMB. As API barite:mMB = 2:1, the thickness was the thinnest and most compact, decreasing by more than 50% under different dosages compared with API barite/WBDFs. The reduction of thickness was 40% at 1:1 and 35% at 1:2. SEM image (Fig. 13(d)) showed that the number and size of pores for mud cake far less than that of API barite/WBDFs. It indicated the wider particle size distribution and the best stacking effect between API barite coarse particles and mMB fine particles at the ratio of 2:1 (Fig. 14(b)). The mud cake was consequently thinner and had excellent quality, and the filtration loss was smaller.

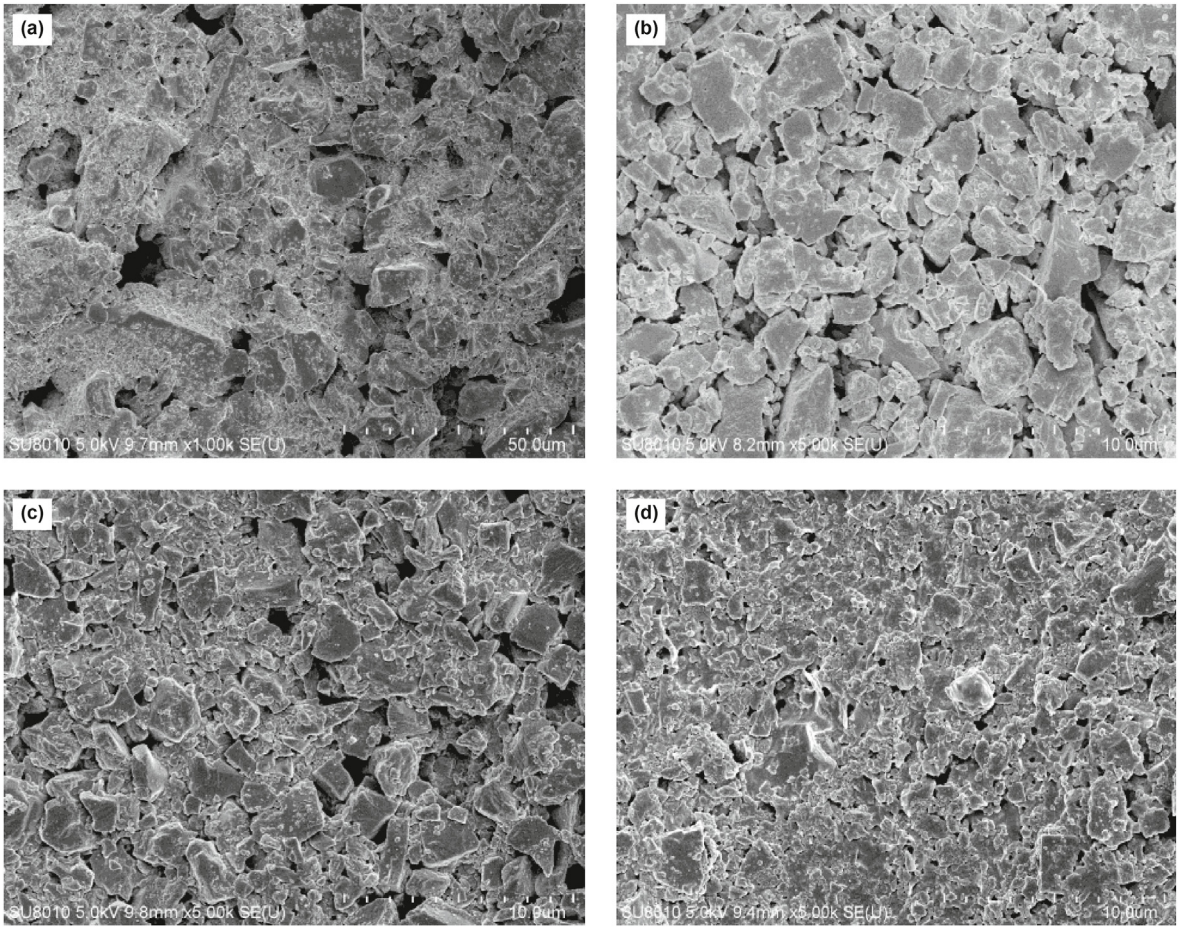

Fig. 13. SEM images of freshly prepared mud cakes of WBDFs weighted with weighting materials after aging at 180 °C for 16 h. (**a**) 600 g of API barite, (**b**) 600 g of MB, (**c**) 600 g of mMB, (**d**) 600 g of API barite:mMB = 2:1.

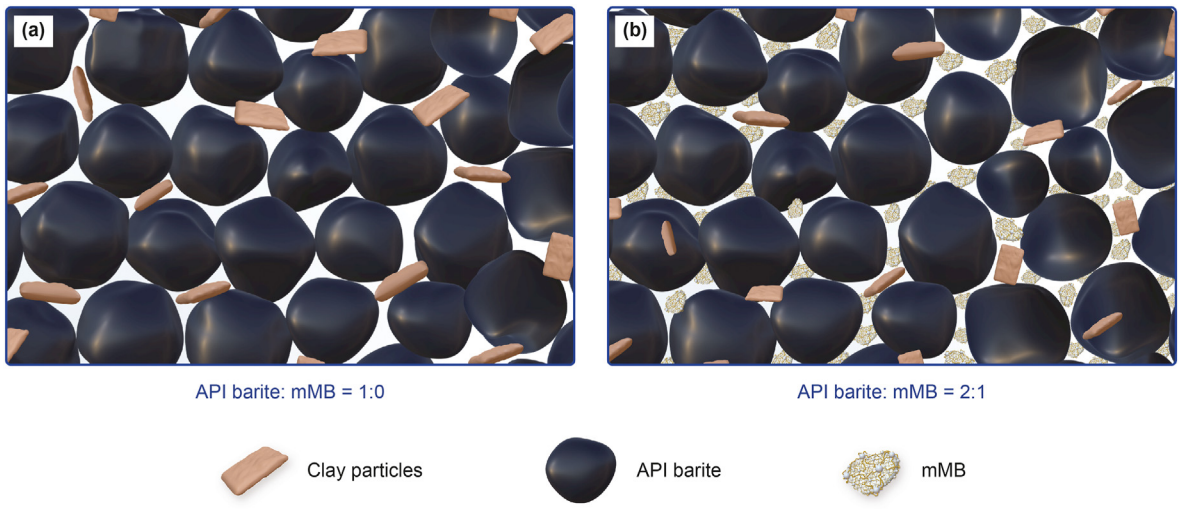

Fig. 14. Particles distributions of mud cakes for WBDFs weighted with weighting materials (**a**) API barite, (**b**) API barite:mMB = 2:1.

Table 5
Lubrication performance of WBDFs weighted with different barites.

Sample, 600 g	Angle, °	Sticking coefficient
WBDFs	3	0.0524
API barite/WBDFs	14.5	0.2443
MB/WBDFs	8.5	0.1495
mMB/WBDFs	9	0.1584
API barite and mMB/WBDFs	6.5	0.1139

3.5.2. Sticking coefficients of mud cakes

The lubrication properties of WBDFs weighted with different barites were evaluated (Table 5). The sticking coefficient of mud cake for API barite/WBDFs was 0.2443, that of MB/WBDFs was 0.1495, by a reduction of 38.8%, and that of mMB/WBDFs was 0.1584, by a reduction of 35.2%, respectively. As API barite and mMB/WBDFs, the sticking coefficient of mud cake was 0.1139, by a reduction of 53.4%. As the mixture of API barite and mMB in WBDFs, the broader particle size distribution and the lubricating effect of fine particles on coarse particles turned out to be more prominent, resulting in the lowest viscosity. Therefore, the combination of mMB and API barite had good lubricity for drilling fluids.

3.5.3. Wear resistance of weighted drilling fluids

The wear resistances of the weighted WBDFs were evaluated using friction coefficients and wear scar diameters (Fig. 15 and Table 6). Generally, the larger the friction coefficient was, the larger the wear scar diameter was. The average friction coefficient of API barite/WBDFs was 0.2987, and the wear scar diameter was 0.784 mm with deep scratches on the steel, due to the irregular and angular surface. The average friction coefficient of mMB/WBDFs was 0.2361, the wear scar diameter was 0.504 mm with thin scratches on the steel. The wear rate decreased with decreasing of the particle size (Saba et al., 2019). The mMB was wrapped with polymer, and the surface was relatively smooth, thereby the wear resistance was improved. As API barite:mMB = 2:1/WBDFs, the average friction coefficient was 0.2603 and the diameter of the wear scar was 0.583 mm, reduced by 13% and 26% compared to API barite. As the addition of mMB, the wear resistance was more significantly improved.

3.6. Reservoir protection performance of WBDFs

We evaluated the reservoir protection performance of WBDFs by comparing the permeability before and after pollution by WBDFs, which was shown in Table 7.

At the beginning of drilling, the mud cake around the wellbore had not yet formed (Shojaei and Ghazanfari, 2022), and the mud invaded into the reservoir instantly (Sun et al., 2018). As drilling continued, the mud cake gradually formed and the filtration loss gradually decreased. It was necessary to quickly form a dense and thin mud cake (Abdou et al., 2018), which could stabilize the wellbore, prevent wellbore leakage and sticking, and prevent filtrate and solid particles from invading the reservoir. The size of solid particles in the mud cake needed to be matched with parameters of pore throat diameter (Wang et al., 2021).

The average particle sizes of API barite, MB and mMB were 21.7, 2.41 and 2.84 μm. The median diameters of pore throat for three cores were 0.623, 0.752, and 0.544 μm. They were smaller than the average diameters of the weighting materials. Therefore, during the pollution process, there was few particles invading into the core. And it formed a dense and thin external mud cake on the core surface, preventing the subsequent invasion of filtrate and finer particles. After a certain pressure blackflow, the mud cake could be removed.

For API barite/WBDFs, it had few particles invading into the reservoir, and the permeability recovery rate after displacement was 81.5%. The recovery rate was 69.6% for API barite:MB = 2:1/WBDFs, indicating severe core damage. The pores of mud cake formed by API barite and MB were large and numerous, and MB particles invaded into the core, and were unable to be removed through displacement. The mud cake was dense and thin formed by API barite:mMB = 2:1/WBDFs. Under the dense accumulation and interaction with clays, the opportunity for mMB to enter the reservoir reduced, and the permeability recovery rate was 87.2% after displacement.

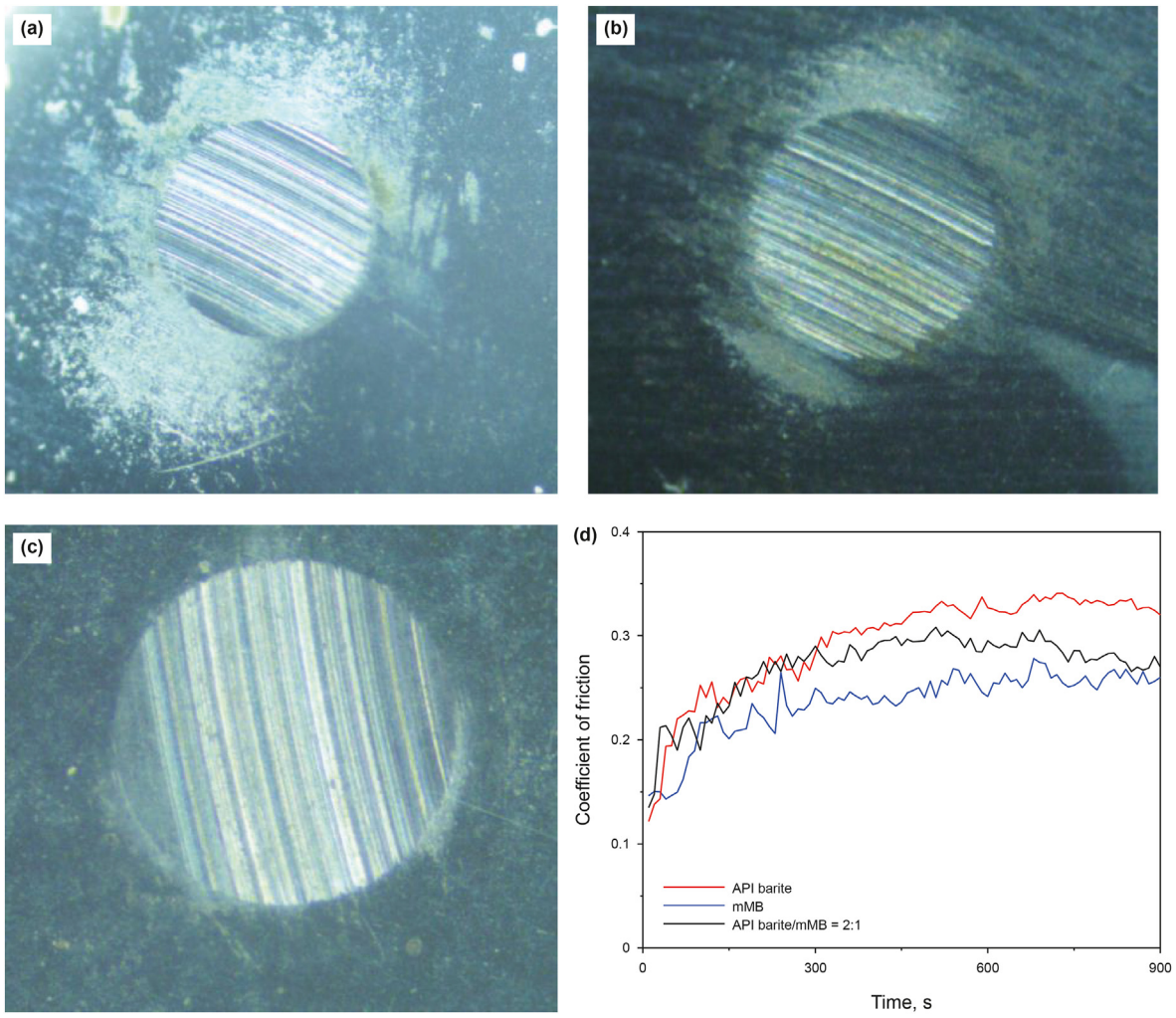

Fig. 15. Digital images of wear scars (**a**) API barite, (**b**) mMB and (**c**) API barite:mMB = 2:1. (**d**) Friction coefficients of WBDFs weighted with different weighting materials.

Table 6
Average friction coefficients and wear scar diameters of WBDFs weighted with different weight materials in 900 s.

Sample	Average friction coefficiency	Wear scar diameter, mm
API barite/WBDFs	0.2987	0.784
mMB/WBDFs	0.2361	0.504
API barite and mMB/WBDFs	0.2603	0.584

Table 7
Permeability and recovery of core damaged by WBDFs weighted by different barites.

Sample	Permeability		
	K_o, mD	K_{od}, mD	K_{od}/K_o
API barite/WBDFs	10.011	8.159	81.5%
API barite and MB = 2:1/WBDFs	4.536	3.159	69.6%
API barite and mMB = 2:1/WBDFs	8.549	7.455	87.2%

4. Conclusion

Micro-sized barite grafted with hydrophilic copolymers was developed for WBDFs in order to balance the formation pressure and prevent reservoir damage in the oil industry. The grafted hydrophilic polymer formed a hydrated film, and increased the electrostatic force and steric hindrance to enhance the dispersion stability. The WBDFs weighted by only mMB showed the highest viscosity and yield point. mMB was also recommended to be added together with API barite at a dosage ratio of 2:1 into WBDFs, decreasing viscosity and simultaneously improving the filtration performance, lubricity, and stability. The dispersion stabilities were enhanced, the mud cake thickness was decreased by 50%, the permeability recovery was recovered, and wear resistance was also improved, compared with API barite only. It was attributed to the suitable particle size distribution, uniform filtration process, and the blocking ability of the mMB, which is mental to achieving a safe, efficient drilling process. Therefore, the chemically modified

weighting materials had a broad application prospect as versatile additives in the extreme conditions of deep and ultra-deep well drilling for oil and gas production.

Author contributions

Lili Yang and Zeyu Liu contributed equally to this work.

Declaration of competing interest

The authors declare that they have no known competing financial interests or personal relationships that could have appeared to influence the work reported in this paper.

Acknowledgments

This work was supported by the National Natural Science Foundation of China (Grant No.51991361) and the foundation of China University of Petroleum (Beijing) (Grant No. 2462021YXZZ002).

Abbreviation

API barite = barite that meets the API standard
mAB = Modified API barite
MB = Micronized barite
mMB = Modified micronized barite
PMADN = P(MSAH/AMPS/DMAA/NVP)
WBDF = water-based drilling fluid
SF = static sag factor
TSI = Turbiscan stability index
HTHP = high-temperature high-pressure

References

Abdou, M.I., Al-Sabagh, A.M., Ahmed, E.S., et al., 2018. Impact of barite and ilmenite mixture on enhancing the drilling mud weight. Egyptian Journal of Petroleum 27 (4), 955–967. https://doi.org/10.1016/j.ejpe.2018.02.004.

Al-Darweesh, J., Aljawad, M.S., Al-Ramadan, M., et al., 2022. Review of underbalanced drilling techniques highlighting the advancement of foamed drilling fluids. J. Pet. Explor. Prod. Technol. 13, 929–958. https://doi.org/10.1007/s13202-022-01596-w.

Almutawa, W., Ahmed, A., Basfar, S., et al., 2021. Investigation of magnetite-based invert emulsion mud at high pressure high temperature. Arabian J. Geosci. 14 (18), 1–8. https://doi.org/10.1007/s12517-021-08293-8.

Ao, T., Yang, L., Xie, C., et al., 2021. Zwitterionic silica-based hybrid nanoparticles for filtration control in oil drilling conditions. ACS Appl. Nano Mater. 4 (10), 11052–11062. https://doi.org/10.1021/acsanm.1c02504.

Basfar, S., Mohamed, A., Elkatatny, S., et al., 2019. A combined barite–ilmenite weighting material to prevent barite sag in water-based drilling fluid. Materials 12 (12), 1945. https://doi.org/10.3390/ma12121945.

Boakye, C., Mahto, V., 2021. Investigating the performance of an organically cross-linked grafted copolymer gel under reservoir conditions for profile modifications in injection wells. J. Sol. Gel Sci. Technol. 97 (1), 71–91. https://doi.org/10.1007/s10971-020-05440-7.

Conn, L., Bruton, J., Rafferty, M., et al., 2007. Unique micronized weight material delivers ultrathin NAF to optimize ERD drilling. In: SPE Annual Technical Conference and Exhibition. Anaheim, California, U.S.A. https://doi.org/10.2118/110584-MS.

Das, D., Mohapatra, R.K., Belbsir, H., et al., 2020. Combined effect of natural dispersant and a stabilizer in formulation of high concentration coal water slurry: experimental and rheological modeling. J. Mol. Liq. 320, 114441. https://doi.org/10.1016/j.molliq.2020.114441.

Delforce, L., Hofmann, E., Nardello-Rataj, V., et al., 2021. TiO_2 nanoparticle dispersions in water and nonaqueous solvents studied by gravitational sedimentation analysis: complementarity of Hansen Parameters and DLVO interpretations. Colloids Surf. A Physicochem. Eng. Asp. 628, 127333. https://doi.org/10.1016/j.colsurfa.2021.127333.

Elkatatny, S., 2019. Mitigation of barite sagging during the drilling of high-pressure high-temperature wells using an invert emulsion drilling fluid. Powder Technol. 352, 325–330. https://doi.org/10.1016/j.powtec.2019.04.037.

Fang, C., Hou, R., Zhou, K., et al., 2014. Surface functionalized barium sulfate nanoparticles: controlled in situ synthesis and application in bone cement. J. Mater. Chem. B 2 (9), 1264–1274. https://doi.org/10.1039/C3TB21544J.

Faraudo, J., Bresme, F., 2005. Origin of the short-range, strong repulsive force between ionic surfactant layers. Phys. Rev. Lett. 94 (7), 077802. https://doi.org/10.1103/PhysRevLett.94.077802.

FelekoğLu, B., 2007. Effects of PSD and surface morphology of micro-aggregates on admixture requirement and mechanical performance of micro-concrete. Cement Concr. Compos. 29 (6), 481–489. https://doi.org/10.1016/j.cemconcomp.2006.12.008.

Gamal, H., Elkatatny, S., Basfar, S., et al., 2019. Effect of pH on rheological and filtration properties of water-based drilling fluid based on bentonite. Sustainability 11 (23), 6714. https://doi.org/10.3390/su11236714.

Gamal, H., Suleymanov, V., Elkatatny, S., et al., 2022. The impact of weighting materials on carbonate pore system and rock characteristics. Can. J. Chem. Eng. 100 (6), 1113–1125. https://doi.org/10.1002/cjce.24092.

Gillani, R., Ercan, B., Qiao, A., et al., 2010. Nanofunctionalized zirconia and barium sulfate particles as bone cement additives. Int. J. Nanomed. 5, 1. https://doi.org/10.2147/IJN.S7603.

Hu, L., Wang, G., Cao, R., et al., 2014. Fabrication and surface properties of hydrophobic barium sulfate aggregates based on sodium cocoate modification. Appl. Surf. Sci. 315, 184–189. https://doi.org/10.1016/j.apsusc.2014.07.068.

Huang, X., Jiang, G., He, Y., et al., 2016. Improvement of rheological properties of invert drilling fluids by enhancing interactions of water droplets using hydrogen bonding linker. Colloids Surf. A Physicochem. Eng. Asp. 506, 467–475. https://doi.org/10.1016/j.colsurfa.2016.07.011.

Huang, Y.M., Zhang, D.Y., Zheng, W.L., 2019. Synthetic copolymer (AM/AMPS/DMDAAC/SSS) as rheology modifier and fluid loss additive at HTHP for water-based drilling fluids. J. Appl. Polym. Sci. 136 (30), 47813. https://doi.org/10.1002/app.47813.

Humood, M., Ghamary, M.H., Lan, P., et al., 2019. Influence of additives on the friction and wear reduction of oil-based drilling fluid. Wear 422, 151–160. https://doi.org/10.1016/j.wear.2019.01.028.

Jeennakorn, M., Alsaba, M., Nygaard, R., et al., 2019. The effect of testing conditions on the performance of lost circulation materials: understandable sealing mechanism. J. Pet. Explor. Prod. Technol. 9 (2), 823–836. https://doi.org/10.1007/s13202-018-0550-4.

Jia, X., Zhao, X., Chen, B., et al., 2022. Polyanionic cellulose/hydrophilic monomer copolymer grafted silica nanocomposites as HTHP drilling fluid-loss control agent for water-based drilling fluids. Appl. Surf. Sci. 578, 152089. https://doi.org/10.1016/j.apsusc.2021.152089.

Jiang, G., Sun, J., He, Y., et al., 2021. Novel water-based drilling and completion fluid technology to improve wellbore quality during drilling and protect unconventional reservoirs. Engineering (11), 129–142. https://doi.org/10.1016/j.eng.2021.11.014.

Kabagire, K.D., Yahia, A., Chekired, M., 2019. Toward the prediction of rheological properties of self-consolidating concrete as diphasic material. Construct. Build. Mater. 195, 600–612. https://doi.org/10.1016/j.conbuildmat.2018.11.053.

Kusrini, E., Oktavianto, F., Usman, A., et al., 2020. Synthesis, characterization, and performance of graphene oxide and phosphorylated graphene oxide as additive in water-based drilling fluids. Appl. Surf. Sci. 506, 145005. https://doi.org/10.1016/j.apsusc.2019.145005.

Leusheva, E., Alikhanov, N., Morenov, V., 2022. Barite-free muds for drilling-in the formations with abnormally high pressure. Fluid 7 (8), 268. https://doi.org/10.3390/fluids7080268.

Li, Z., Zhao, G., Xiang, C., 2022. Synthesis and properties of a gel agent with a high salt resistance for use in weak-gel-type water-based drilling fluid. Arabian J. Sci. Eng. 47 (9), 12045–12055. https://doi.org/10.1007/s13369-022-06826-1.

Liu, Y., Zhang, Y., Yan, J., et al., 2019. Application of thermal resistant gemini surfactants in highly thixotropic water-in-oil drilling fluid system. Open Chem. 17 (1), 1435–1441. https://doi.org/10.1515/chem-2019-0157.

Liu, J., Dai, Z., Xu, K., et al., 2020. Water-based drilling fluid containing bentonite/poly (sodium 4-styrenesulfonate) composite for ultrahigh-temperature ultra-deep drilling and its field performance. SPE J. 25 (3), 1193–1203. https://doi.org/10.2118/199362-PA.

Liu, H., Cui, S., Meng, Y., et al., 2021. Rock mechanics and wellbore stability of deep shale during drilling and completion processes. J. Petrol. Sci. Eng. 205, 108882. https://doi.org/10.1016/j.petrol.2021.108882.

Liu, J., Liu, J., Zhong, J., et al., 2021. Preparation of graphene oxide/attapulgite composites and their demulsification performance for oil-in-water emulsion. Energy Fuels 35 (6), 5172–5180. https://doi.org/10.1021/acs.energyfuels.1c00042.

Mahmoud, H., Hamza, A., Nasser, M.S., et al., 2020. Hole cleaning and drilling fluid sweeps in horizontal and deviated wells: comprehensive review. J. Petrol. Sci. Eng. 186, 106748. https://doi.org/10.1016/j.petrol.2019.106748.

Mao, H., Yang, Y., Zhang, H., et al., 2020. Conceptual design and methodology for rheological control of water-based drilling fluids in ultra-high temperature and ultra-high pressure drilling applications. J. Petrol. Sci. Eng. 188, 106884. https://doi.org/10.1016/j.petrol.2019.106884.

Morenov, V., Leusheva, E., Martel, A., 2018. Investigation of the fractional composition effect of the carbonate weighting agents on the rheology of the clayless drilling mud. Int. J. Eng. 31 (7), 1152–1158. https://doi.org/10.5829/ije.2018.31.07a.21.

Murtaza, M., Tariq, Z., Mahmoud, M., et al., 2021. Anhydrite (calcium sulfate) mineral as a novel weighting material in drilling fluids. J. Energy Resour. Technol. 143 (2), 023002. https://doi.org/10.1115/1.4047762.

Navarrete, I., Kurama, Y., Escalona, N., et al., 2022. Effect of supplementary cementitious materials on viscosity of cement-based pastes. Cement Concr. Res.

151, 106635. https://doi.org/10.1016/j.cemconres.2021.106635.
Razmjou, A., Mansouri, J., Chen, V., 2011. The effects of mechanical and chemical modification of TiO2 nanoparticles on the surface chemistry, structure and fouling performance of PES ultrafiltration membranes. J. Membr. Sci. 378 (1–2), 73–84. https://doi.org/10.1016/j.memsci.2010.10.019.
Ren, Y., Zheng, J., Xu, Z., et al., 2018. Application of Turbiscan LAB to study the influence of lignite on the static stability of PCLWS. Fuel 214, 446–456. https://doi.org/10.1016/j.fuel.2017.08.026.
Saba, Farhad, Zhang, F., Liu, S., et al., 2019. Reinforcement size dependence of mechanical properties and strengthening mechanisms in diamond reinforced titanium metal matrix composites. Compos. B Eng. 167, 7–19. https://doi.org/10.1016/j.compositesb.2018.12.014.
Shimpi, N., Mali, A., Hansora, D.P., et al., 2015. Synthesis and surface modification of calcium carbonate nanoparticles using ultrasound cavitation technique. Nanoscience and Nanoengineering 3 (1), 8–12. https://doi.org/10.13189/nn.2015.030102.
Shojaei, N., Ghazanfari, M.H., 2022. Reduction of formation damage in horizontal wellbores by application of nano-enhanced drilling fluids: experimental and modeling study. J. Petrol. Sci. Eng. 210, 110075. https://doi.org/10.1016/j.petrol.2021.110075.
Sun, S., Ding, H., Zhou, H., 2017. Preparation of TiO_2-coated barite composite pigments by the hydrophobic aggregation method and their structure and properties. Sci. Rep. 7 (1), 1–12. https://doi.org/10.1038/s41598-017-10620-7.
Sun, J., Ning, F., Lei, H., et al., 2018. Wellbore stability analysis during drilling through marine gas hydrate-bearing sediments in Shenhu area: a case study. J. Petrol. Sci. Eng. 170, 345–367. https://doi.org/10.1016/j.petrol.2018.06.032.
Tang, Z., Qiu, Z., Zhong, H., et al., 2022. Novel acrylamide/2-acrylamide-2-3 methylpropanesulfonic acid/styrene/maleic anhydride polymer-based $CaCO_3$ nanoparticles to improve the filtration of water-based drilling fluids at high temperature. Gels 8 (5), 322. https://doi.org/10.3390/gels8050322.
Tian, Y., Wu, Y., Wang, Z., et al., 2019. Fe_3O_4/poly (acrylic acid) nanoparticles as modifiers for improving rheological and filtration properties of water-based drilling fluids. J. Macromol. Sci., Part A 56 (5), 393–402. https://doi.org/10.1080/10601325.2019.1578619.
Ulusoy, U., 2019. Quantifying of particle shape differences of differently milled barite using a novel technique: dynamic image analysis. Materialia 8, 100434. https://doi.org/10.1016/j.mtla.2019.100434.
Wagle, V., Al-Yami, A.S., Aljubran, M., et al., 2018. High density drilling fluids for managed pressure drilling. In: SPE Kingdom of Saudi Arabia Annual Technical Symposium and Exhibition. Dammam, Saudi Arabia. https://doi.org/10.2118/192248-MS.
Wang, J., Xiong, Y., 2022. Research and application of high-density cementing slurry technology under the condition of oil-based drilling fluid in salt formation. Arabian J. Sci. Eng. 47 (6), 7069–7079. https://doi.org/10.1007/s13369-021-06325-9.
Wang, B., Sun, J., Shen, F., et al., 2020. Mechanism of wellbore instability in continental shale gas horizontal sections and its water-based drilling fluid countermeasures. Nat. Gas. Ind. B 7 (6), 680–688. https://doi.org/10.1016/j.ngib.2020.04.008.
Wang, Z., Li, Z., Fu, S., et al., 2021. Experimental study of the plugging–matching relationship between elastic particles and formation pore throats. J. Dispersion Sci. Technol. 42 (2), 190–205.
Wang, D., Qiu, Z., Zhong, H., et al., 2022. Performance control of high temperature and high density drilling fluid based on fractal grading theory. Geoenergy Science and Engineering 211377. https://doi.org/10.1016/j.geoen.2022.211377.
Wu, J.Y., Liu, Q.L., Xiong, Y., et al., 2009. Molecular simulation of water/alcohol mixtures' adsorption and diffusion in zeolite 4A membranes. J. Phys. Chem. B 113 (13), 4267–4274. https://doi.org/10.1021/jp805923k.
Wu, J., He, J., Torsater, O., et al., 2012. Effect of nanoparticles on oil-water flow in a confined nanochannel: a molecular dynamics study. In: SPE International Oilfield Nanotechnology Conference and Exhibition. Noordwijk, The Netherlands. https://doi.org/10.2118/156995-MS.
Xu, D.S., Tang, J.Y., Zou, Y., et al., 2019. Macro and micro investigation of gravel content on simple shear behavior of sand-gravel mixture. Construct. Build. Mater. 221, 730–744. https://doi.org/10.1016/j.conbuildmat.2019.06.091.
Zhang, X., Jiang, G., Xuan, Y., et al., 2017. Associating copolymer acrylamide/diallyldimethylammonium chloride/butyl acrylate/2-acrylamido-2-methylpropanesulfonic acid as a tackifier in clay-free and water-based drilling fluids. Energy Fuels 31 (5), 4655–4662. https://doi.org/10.1021/acs.energyfuels.6b02599.
Zou, H., Wu, S., Shen, J., 2008. Polymer/silica nanocomposites: preparation, characterization, properties, and applications. Chem. Rev. 108 (9), 3893–3957. https://doi.org/10.1021/cr068035q.